JOURNAL OF SOLID STATE CHEMISTRY 116, 53–60 (1995)

Double Cationic Ordering in the "1201" Substituted Type Cuprate $HgBiSr_7Cu_2SbO_{15}$

D. Pelloquin, M. Hervieu, C. Michel, M. Caldes,* and B. Raveau

Laboratoire CRISMAT, CNRS URA 1318-ISMRA, Université de Caen Boulevard du Maréchal Juin, 14050 Caen Cedex, France; and
**Institute de Ciencia de Materials de Barcelona, Campus UAB, 08193 Bellaterra, Spain*

Received March 10, 1994; in revised form August 30, 1994; accepted September 6, 1994

A new substituted cuprate, $HgBiSr_7Cu_2SbO_{15}$, has been isolated; its structure has been determined by powder X-ray diffraction and high resolution electron microscopy. It crystallizes in the orthorhombic system with $a = 7.6799(5)$ Å $\approx 2a_p$, $b = 11.5549(7)$ Å $\approx 3a_p$, $c = 8.8795(4)$ Å $\approx c_{1201}$. This structure belongs to the 1201 type family, i.e., consists of single perovskite octahedral layers intergrown with double rock salt layers. But its originality deals with a double cationic 1:2 ordering in the $SbCu_2$ perovskite layers and Sr(Hg, Bi)$_2$ rock salt layers, leading to the formulation $([(Hg, Bi)_2][SrO_3][Sr_3O_3])_{RS}(Sr_3Cu_2SbO_9)_P$. This correlated ordering between two kinds of layers is explained in terms of the size of the different metallic elements. The microstructural study shows that other types of ordering are observed locally in the matrix.

INTRODUCTION

After the discovery of superconductivity at high temperature in copper oxides (1), the exploration of copper-based systems has shown the existence of a tremendous number of cuprates that consist of intergrowths of perovskite type layers, oxygen deficient or not, with more or less distorted multiple rock salt type layers (see for a review Ref. (2)). The remarkable flexibility of such structures allows several metallic elements to be introduced in the same rock salt layer simultaneously. This is the case for the recently discovered mercury-based cuprates $HgBa_2Ca_{m-1}Cu_mO_{2m+2}$ (3–6), in which isovalent or aliovalent substitutions allowed more than 15 new cuprates to be stabilized (7–18). But the mercury cuprates differ from other cuprates by their ability to exhibit cationic orderings in the mixed rock salt layers. This phenomenon has been evidenced between praseodymium and mercury in the 1201, 1212, and 1222 cuprates (10, 13, 18). On the other hand, no ordered substitution on the copper sites of the mercury cuprates has been reported to date. We have thus considered the possible substitution of various elements for copper in the sample 1201 structure $Hg_{0.5}Bi_{0.5}Sr_2CuO_{5-\delta}$ (9) that is characterized by a random distribution of mercury and bismuth in the $[Bi_{0.5}Hg_{0.5}O_{1-\delta}]_\infty$ layer. We report here on a new phase, $HgBiSr_7Cu_2SbO_{15}$, that exhibits a double cationic ordering in the 1201 type structure.

EXPERIMENTAL

Samples with nominal composition $(Hg_{0.5}Bi_{0.5})_{1-x}Sr_{2+x}Cu_{1-y}Sb_yO_5$ were prepared from mixtures of HgO, Bi_2O_3, Sb_2O_3, SrO_2, and CuO, intimately ground in an agate mortar. They were slowly heated in a quartz tube up to 900°C; after a plateau of several hours, the temperature was slowly decreased to room temperature.

X-ray diffraction data were collected by means of a Philips vertical diffractometer (Cu$K\alpha$ radiation), in the range $7 \leq 2\theta \leq 70°$ by step scanning with an increment of 0.02° (2θ). The lattice constants and structure were calculated using the Rietveld method (program DBW3-2 (19)). The electron diffraction study was carried out on a JEOL 200 CX microscope fitted with an eucentric goniometer (±60°). High resolution microscopy (HREM) was performed with a TOPCON 002B microscope, operating at 200 kV and having a point resolution of 1.8 Å. The EDS analysis was performed with a Kevex analyzer. The crystals were crushed in alcohol and flakes deposited on a holey carbon film supported by an aluminum grid.

RESULTS AND DISCUSSION

Structure of $HgBiSr_7Cu_2SbO_{15}$

For the above experiment, a single phase is obtained for $x = y \approx 1/3$, i.e., leading to the composition $HgBiSr_7Cu_2SbO_{15}$. The powder X-ray diffraction analysis evidences a 1201 type structure with weak extra reflections (Fig. 1).

The electron diffraction study confirms that the basic reflections are those of a 1201 type subcell but, as shown from the basic sections [001], [010], and [100] (Fig. 2), one observes extra reflections that indicate a

0022-4596/95 $6.00

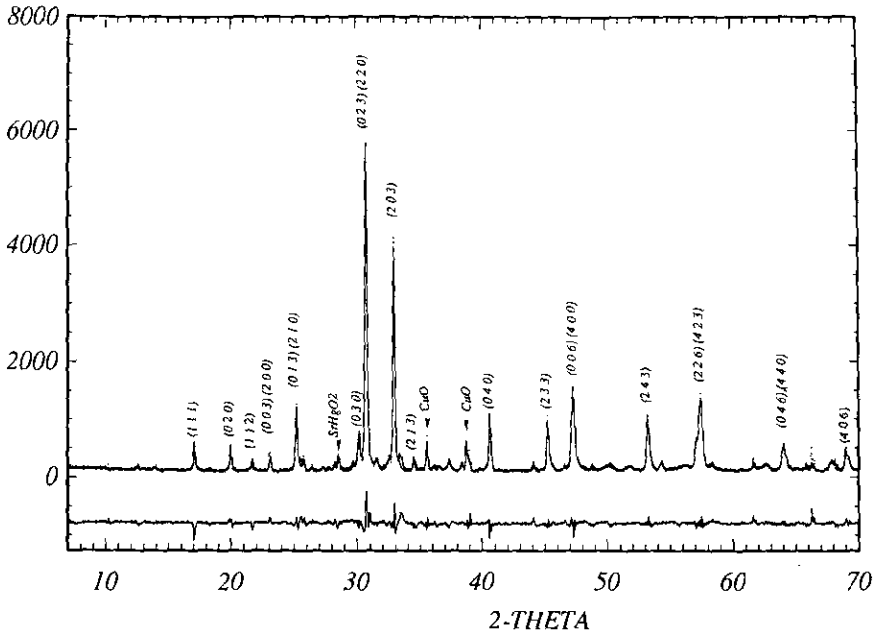

FIG. 1. Powder X-ray diffraction of $HgBiSr_7Cu_2SbO_{15}$.

doubling of the a parameter and a tripling of the b parameter. The cell symmetry is orthorhombic and the reflection conditions are $h0l$, $h = 2n$ leading to the possible space groups $Pma2$ and $Pmam$. The lattice parameters of the orthorhombic cell, refined from the powder X-ray data, are

$$a = 7.6799(5)\ \text{Å} \approx 2a_p; \quad b = 11.5549(7)\ \text{Å} \approx 3a_p; \quad c = 8.8795(4)\ \text{Å} \approx c_{1201}.$$

The EDS analysis performed on 20 crystals shows that the actual cationic composition is practically constant and close to the nominal composition, i.e., $Hg_{1.05}Bi_{1.05}Sr_{6.9}Cu_2Sb$. Note that the consideration of the charge balance, taking the different elements as Hg(II), Bi(III), Cu(II), and Sb(V), leads to the ideal O_{15} composition expected for a fully oxygenated 1201 structure.

Taking into consideration the size of the metallic elements and their usual coordination, it appears likely that copper and antimony are located in the same octahedral layer, whereas the intermediate rock salt layer may contain mercury, bismuth, and strontium simultaneously, according to the formula $(HgBiSr)Sr_6(Cu_2Sb)O_{15}$. If this is the case, one should observe three kinds of metallic layers: mixed Hg, Bi, Sr, pure Sr, and mixed Cu_2Sb stacked along **c**. The HREM images (Fig. 3a) recorded along [010] confirm without ambiguity this hypothesis. For a focus value close to -20 nm, the cations appear as black dots. One indeed observes three rows of staggered more intense black dots (arrowheads) that can be correlated to two Sr and one SrHgBi layers, respectively and one row of less intense black spots of gray spots (small arrows) that are correlated to one CuSb layer. Thus the stacking of these rows along **c** is in agreement with the stacking sequence of the layers,

$$[(Cu, Sb)O_2]_\infty\text{–}[SrO]_\infty\text{–}[(Hg, Bi, Sr)O]_\infty\text{–}[SrO]_\infty,$$

that characterizes the 1201 classical structure (Fig. 3b).

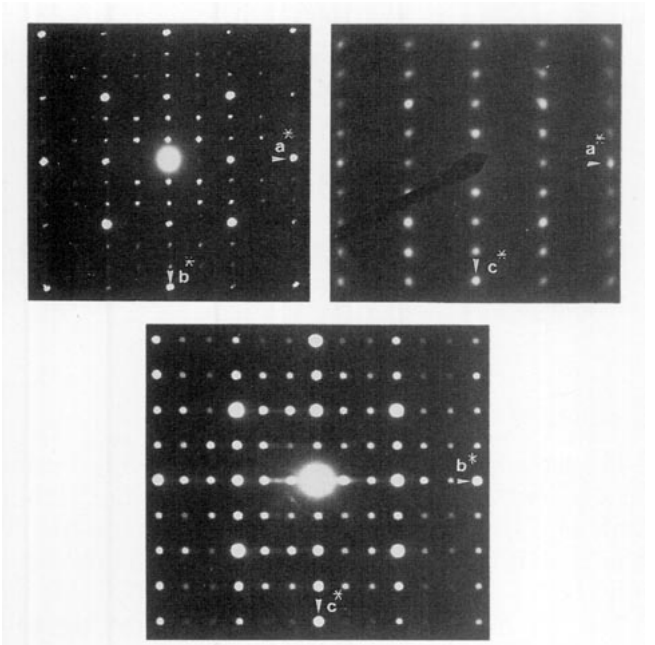

FIG. 2. (a) [001] (b) [010], and (c) [100] electron diffraction patterns of the phase $HgBiSr_7Cu_2SbO_{15}$.

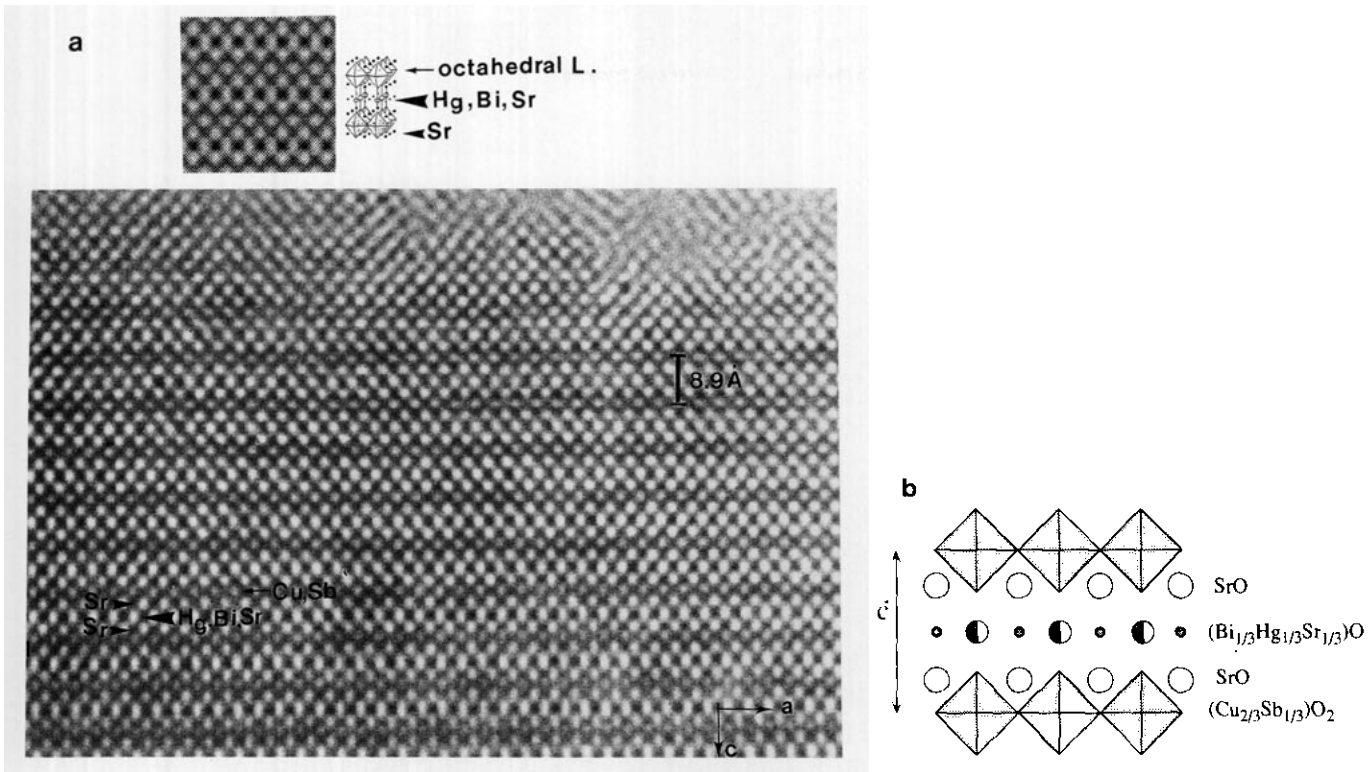

FIG. 3. (a) [010] HREM image of $HgBiSr_7Cu_2SbO_{15}$. Along that direction the ordering phenomena cannot be evidenced, since the different cations (noted on the image) are cast on the same point. The calculated image (Δf = 20 nm, t = 31 Å) is compared to the experimental one and to the model. (b) Idealized drawing of the structure of $HgBiSr_7Cu_2SbO_{15}$ projected along [010]; it corresponds to a classical "1201" structure.

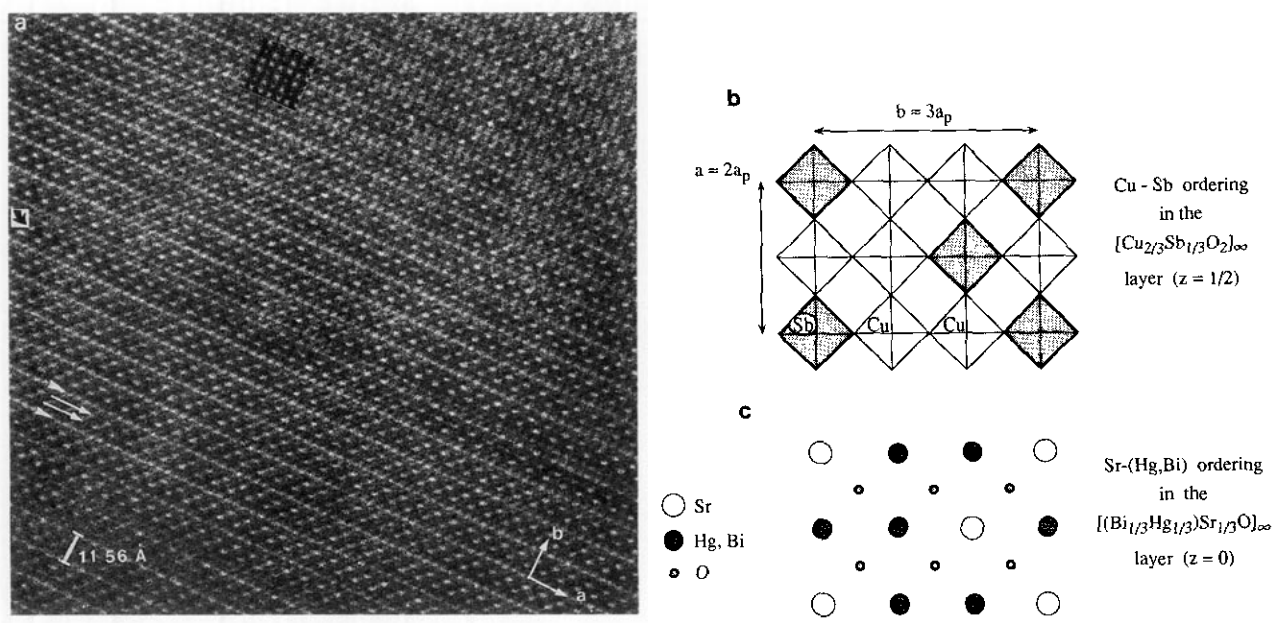

FIG. 4. (a) [001] HREM image of $HgBiSr_7Cu_2SbO_{15}$ where the cationic positions are highlighted. A direct correlation with the nature of the cations cannot be made because the atoms of two mixed layers "HgBiSr" and "Cu_2Sb" are superimposed along that direction. However, this image allows a model of ordering to be proposed. The arrowheads and straight arrows differentiate the two types of layers. The curved arrow shows a defect where the periodicity along **b** is 4 × a_p. The calculated image for Δf = 20 nm and thickness = 124 Å is superposed on the image in the upper part of the figure. (b) Idealized model of the ordering in the "Cu_2Sb" layer. (c) Idealized model of the ordering in the "HgBiSr" layer.

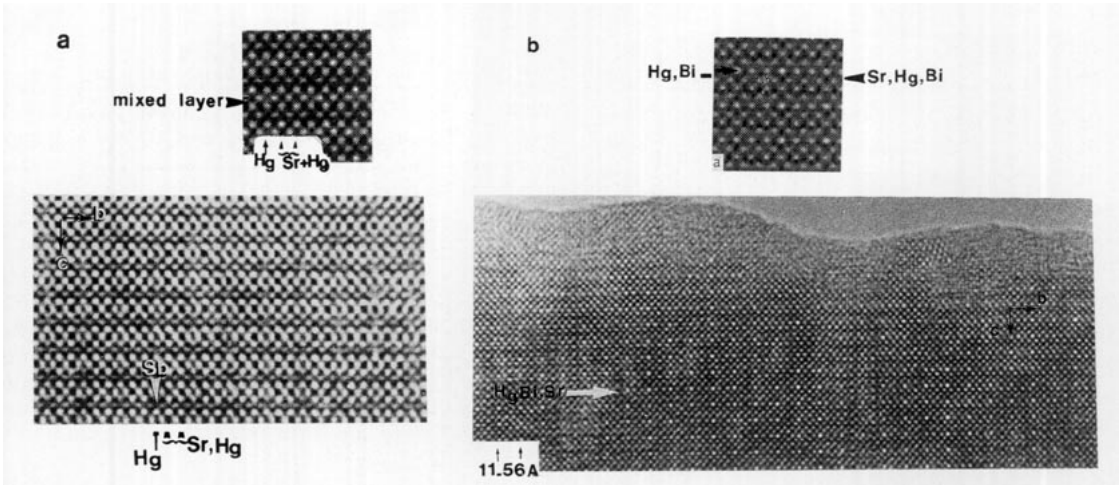

FIG. 5. [100] HREM images: (a) for a focus value close to −5 nm where the positions of the cations appear as dark dots. One cation of the "HgBiSr" layer (black arrowhead) out of three is surrounded by four closer white dots whereas, just below, the cation of the "Cu_2Sb" layer (white arrowhead) is surrounded by four more distant white dots; (b) for a focus value of −45 nm, where the positions of the cations appear as white dots. The corresponding calculated images are compared (above the experimental images) in both cases (thickness = 31 Å) and the cations are noted.

The examination of the [001] images, allows for particular defocus values the ordering phenomena to be evidenced as shown in Fig. 4a where the cationic positions are highlighted. One indeed observes a sequence of one row of bright dots spaced of 3.8 Å running along **a** (arrowheads), which alternates with two rows of staggered white dots (straight arrows) spaced 7.6 Å apart. This suggests that an ordering appears in the (001) layers, either between copper and antimony, or between bismuth, mercury, and strontium, or in both kinds of layers. The two corresponding possible orderings are schematized in Figs. 4b–4c. In the $[(Cu_2Sb)O_6]_\infty$ layers (Fig. 4b), one SbO_6 octahedron alternates with two CuO_6 octahedra along **b**, forming $[Cu_2SbO_9]_\infty$ chains; along **a** two successive $[Cu_2SbO_9]_\infty$ chains are shifted a_p with respect to each other in agreement with the staggered configuration of the white dots, leading to a doubling of the a parameter. The $[(Hg, Bi)_2SrO_3]_\infty$ layers may exhibit a similar ordering (Fig. 4c), taking into consideration the ability of bismuth and mercury to be distributed statistically on the same crystallographic site; thus two heavy cations (bismuth or mercury) alternate with one strontium ion along **b**, forming $[(Bi, Hg)_2SrO_3]_\infty$ rows; two successive rows are then shifted of a_p, so that a doubling of the a parameter is obtained (Fig. 4c).

The [100] images (Fig. 5) show that the ordering appears on the two kinds of layers Cu_2Sb and HgBiSr. In the enlarged image of Fig. 5a where cations appear as black dots, one indeed observes at the level of the mixed mercury layers HgBiSr (black arrowhead) a sequence of two intense dark spots, followed by smaller one, the latter being closely surrounded by four white spots; just below, in octahedral layer, the corresponding cation position is surrounded by four more distant white dots (white arrowhead). In another view, in Fig. 5b where the cations are highlighted (Δf = −45 nm), a bright dot is observed every three dots at the level of the mixed layer (straight white arrows). Thus this confirms that in the $[(Hg, Bi)_2SrO_3]_\infty$ layer, one [100] row of heavy ions (Hg or Bi) alternates with two [100] mixed rows of ions (Hg_2Sr or Bi_2Sr) in agreement with the ordered model proposed for this layer (Fig. 4c). In the thicker part of the crystals, the contrast evidences the second ordering phenomena (Fig. 6) at the level of the

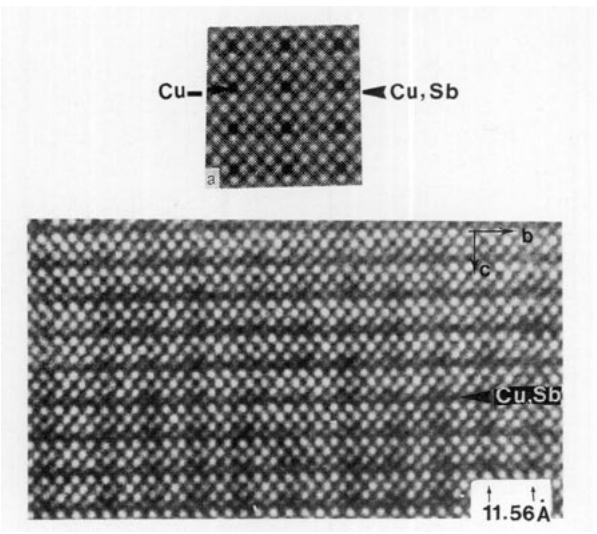

FIG. 6. [100] HREM image recorded in the thicker part of the crystal (Δf = 10 nm, thickness = 124 Å), the ordering phenomena is clearly observed at the level of the octahedral layer. Such an effect is assumed to be introduced by a local change in the cation environment.

copper–antimony layers in agreement with the proposed model (Fig. 4b). One indeed observes that one dark spot (cation positions) of the octahedral layer out of three is surrounded by four white dots (anion positions) which are wider apart than those surrounded the two other dark spots. Such an effect is supposed to be induced essentially by changes in the cation environment, especially due to size variations.

Thus, these observations establish that the cationic ordering appears in the two kinds of layers, octahedral $[Cu_2SbO_6]_\infty$ layers and $[(Hg, Bi)_2SrO_3]_\infty$ layers.

In order to confirm this cationic distribution in the 1201 ordered structure, calculations were carried out from powder X-ray data. The starting positional parameters were deduced from the parent oxide $Hg_{0.5}Bi_{0.5}Sr_2CuO_{5-\delta}$ (9), using the model of the cationic ordering described in Figs. 4b–4c. The most symmetric space group, *Pmam*, was chosen first. The positional parameters were first refined, then the occupancy factors of heavy atoms, and last the thermal factors. In each layer, a unique anisotropic B factor was refined for all the heavy atoms of one layer, whereas all the B factors of the oxygen atoms were fixed to 1 Å^2 in order to limit the number of variable parameters. The R_I factor was lowered to 0.075 for the atomic coordinates listed in Table 1. These results confirm the 1:2 ordering observed along **a** for both kind of layers $SbCu_2$ and $Sr(Hg, Bi)_2$. In particular, all attempts to introduce Sb on the Cu sites, or Hg (or Bi) on the Sr sites, lead to a significant increase of the reliability factor.

TABLE 1

Positional Parameters of $HgBiSr_7Cu_2SbO_{15}$ (Space Group, *Pmam*, a = 7.6799(5) Å; b = 11.5549(7) Å; c = 8.8795(4) Å R_p = 10.15%; R_{wp} = 14.17%; R_I = 6.5%; χ^2 = 4.83)

Atoms	Site	x	y	z	B (Å^2)	τ
Sr1	2*e*	0.25	0.163(3)	0.0	0.61(8)[a]	1
Bi1	2*e*	0.25	0.5	0.0	0.61(8)[a]	0.5
Hg1	2*e*	0.25	0.5	0.0	0.61(8)[a]	0.5
Bi2	2*e*	0.75	0.170(1)	0.0	0.61(8)[a]	0.5
Hg2	2*e*	0.75	0.170(1)	0.0	0.61(8)[a]	0.5
Sr2	4*g*	0.0	0.0	0.2903(4)	0.08(6)[b]	1[c]
Sr3	8*l*	0.0	0.343(1)	0.1903(4)	0.08(6)[b]	1[c]
Sb	2*e*	0.25	0.182(2)	0.5	0.22(8)[d]	1[c]
Cu1	2*e*	0.25	0.5	0.5	0.22(8)[d]	1[c]
Cu2	2*e*	0.75	0.167(4)	0.5	0.22(8)[d]	1[c]
O1	2*a*	0.0	0.0	0.0	1.00[c]	1[c]
O2	4*g*	0.0	0.334(3)	0.0	1.00[c]	1[c]
O3	4*k*	0.75	0.164(4)	0.232(2)	1.00[c]	1[c]
O4	4*k*	0.25	0.105(4)	0.294(1)	1.00[c]	1[c]
O5	4*k*	0.25	0.5	0.232(2)	1.00[c]	1[c]
O6	2*f*	0.25	0.0	0.5	1.00[c]	1[c]
O7	4*j*	0.0	0.167(3)	0.5	1.00[c]	1[c]
O8	2*d*	0.0	0.5	0.5	1.00[c]	1[c]
O9	2*f*	0.25	0.340(4)	0.5	1.00[c]	1[c]
O10	2*f*	0.75	0.333(4)	0.5	1.00[c]	1[c]

[a] Refined together.
[b] Refined together.
[c] Not refined.
[d] Refined together.

At this stage of the investigation, theoretical images were calculated for thicknesses ranging from 3.1 to 124 nm; the ordering hypothesis is confirmed. Images along [100] for a thickness of 7.7 nm are reproduced in Fig. 7 as an example. Note that the difference in contrast at the level of the Sb and Cu atoms is hardly visible, as in the experimental images. In order to check the origin of such a contrast, calculations were performed substituting Cu for Sb, i.e., considering a pure copper $[CuO_2]_\infty$ layer, without changing the oxygen positions. The contrast remains unchanged; this shows that the contrast in these ordered structure arises also from the oxygen displacements due to the cation ordering. The calculated images are compared to the experimental ones in Figs. 3 to 6.

The observation of the [100] images shows that a nonsymmetrical contrast is observed at the level of the positions of the two atoms O_3 and O_4, i.e., corresponding to the two oxygen atoms of the $[SrO]_\infty$ layers, located at the level of Sr of the mixed $[(Hg, Bi)_2SrO_3]_\infty$ layer. This systematic effect, dealing only with one type of atom, has been shown to be independent of tilted or bent areas of the crystals; it can be attributed to an atom displacement. Two independent positions for O_3 and O_4 imply a loss of the mirror m and then, to consider a *Pma*2 space group. Structural calculations performed in the space group *Pma*2 lead to a significant decrease of the R_I value to 0.065; in the same way, the corresponding HREM calculations confirm that such a nonsymmetry leads to a variation in contrast similar to that observed. However, taking into account the complexity of the structure, it appears unreasonable to consider as significant the oxygen positions.

Thus the structure of $HgBiSr_7Cu_2SbO_{15}$ (Fig. 8) consists of single octahedral perovskite layers $[Sr_3Cu_2SbO_9]_\infty$ characterized by a 1:2 ordering of the CuO_6 and SbO_6 octahedra, intergrown with double rock salt type layers whose middle $[HgBiSrO_3]_\infty$ layers are also characterized by a 1:2 ordering of the SrO_6 octahedra and BiO_6 or HgO_6 octahedra. In fact, from the three-dimenional structure (Fig. 8), it is clear that the two kinds of ordering are correlated. The interatomic distances (Table 2) are in agreement with those generally observed in the cuprate- and mercury-based compounds and with ionic radii given by Shannon (20). One indeed observes that the SbO_6 octahedra that are smaller are connected to the SrO_6 octahedra (average distance Sb–O = 1.97 Å) that are the largest, along **c**, whereas the CuO_6 octahedra (average distance Cu–O = 2.06 Å) that exhibit

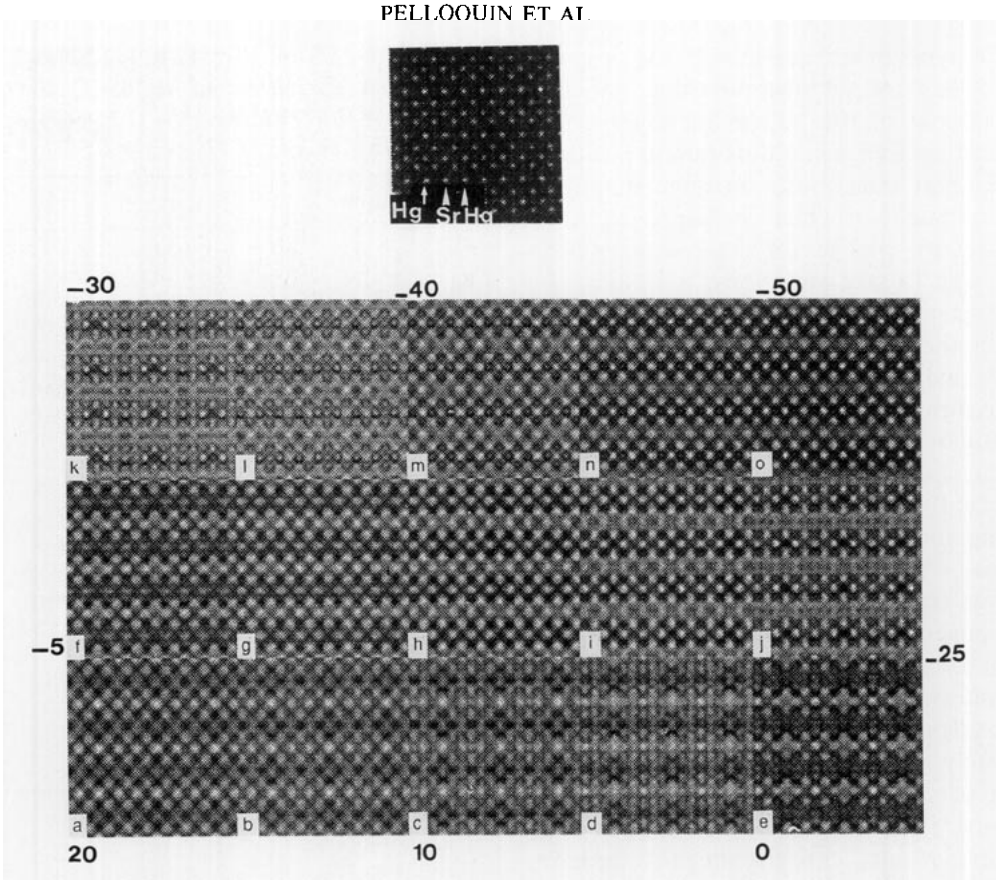

FIG. 7. Example of calculated through-focus series for a crystal thickness of 77 Å; the focus value is indicated (from 20 to −50 Å by 5-Å steps). The projected potential is shown in the upper part.

long Cu–O apical distances are connected to the HgO_6 or BiO_6 octahedra whose Bi–O bonds are significantly smaller than the Sr–O distances.

Deviation from the Perfect Ordering

The first important point deals with the highly regular stacking of the layers along **c**, according to a 1201 mode, as shown from numerous [010] HREM images. This is not the case for the cationic ordering within the mixed Cu_2Sb and $(Hg, Bi)_2Sr$ [001] layers, where several types of local ordering have been observed.

Variation of the local ordering without modification of the stoichiometry. The first phenomenon is observed on [001] images, where the alternation of gray (Hg, Bi) and white (Sr) dots in staggered positions is not perfectly ensured (Fig. 9a). In some areas, the contrast is less pronounced (left part of the image). This can be explained by a translation of $a/2$ of two successive $[(Hg, Bi)_2SrO_3]_\infty$ layers as illustrated on Fig. 9b. The superimposition of $a/2$ shifted $[(Hg, Bi)_2SrO_3]_\infty$ layers leads indeed to the formation of a quite even contrast and implies the existence of a (010) mirror plane at the level of the Hg(Bi) rows. Note that such a local variation of the ordering does not modify the contrast along [100]. Moreover it cannot be detected in the ED patterns since the new periodicity of the local structure is smaller than that of the matrix, i.e., "$a_p \times 3a_p \times c_{201}$."

A second effect, dealing with the modification of the contrast of staggered spots is also observed on [001] im-

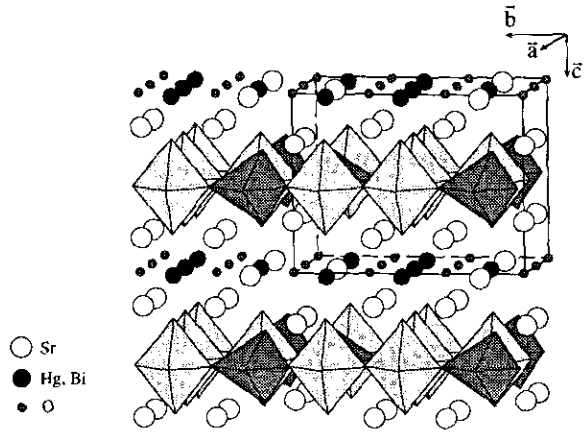

FIG. 8. Structure of $HgBiSr_7Cu_2SbO_{15}$.

TABLE 2
Interatomic Distances (Å)

$(Hg, Bi)_1$–O_2	2.71(2)	× 4
$(Hg, Bi)_1$–O_5	2.06(2)	× 2
$(Hg, Bi)_2$–O_2	2.75(1)	× 2
$(Hg, Bi)_2$–O_2	2.69(2)	× 2
$(Hg, Bi)_2$–O_5	2.06(2)	× 2
Sr_1–O_1	2.68(2)	× 2
Sr_1–O_2	2.75(3)	× 2
Sr_1–O_4	2.69(1)	× 2
Sr_2–O_1	2.578(4)	× 1
Sr_2–O_3	2.74(3)	× 2
Sr_2–O_4	2.27(2)	× 2
Sr_2–O_6	2.675(2)	× 2
Sr_2–O_7	2.68(2)	× 2
Sr_3–O_3	2.86(3)	× 1
Sr_3–O_5	2.694(8)	× 2
Sr_3–O_4	3.34(4)	× 1
Sr_3–O_2	2.58(4)	× 1
Sr_3–O_7	2.75(3)	× 1
Sr_3–O_8	2.603(8)	× 1
Sr_3–O_9	2.675(2)	× 1
Sr_3–O_{10}	2.677(3)	× 1
Sb–O_4	2.03(2)	× 2
Sb–O_7	1.927(4)	× 2
Sb–O_6	2.10(2)	× 1
Sb–O_9	1.83(5)	× 1
Cu_1–O_5	2.37(2)	× 2
Cu_1–O_8	1.920	× 2
Cu_1–O_9	1.85(5)	× 1
Cu_1–O_{10}	1.92(5)	× 1
Cu_2–O_3	2.37(2)	× 2
Cu_2–O_7	1.920	× 2
Cu_2–O_6	1.93(5)	× 1
Cu_2–C_{10}	1.91(6)	× 1

ages (large arrow). At the level of this defect the shifting of two successive [100] rows of white spots is no longer consistent; the contrast consists locally in two adjacent rows of alternated white and gray dots. This is easily explained (Fig. 9c) by the fact that in each $[(Hg, Bi)_2SrO_3]_\infty$ layer one [100] Hg, Bi, Sr mixed layer out of two is translated of $a/2$, i.e., a_p. As a result the periodicity $2a_p \times 3a_p \times c_{1201}$ is not modified but the local symmetry has changed to *Pmmm* (or *Pmm*2).

Variation of the local stoichiometry. One frequent defect is a variation of the periodicity along **b**; instead of the expected $3 \times a_p$ superstructure one observes local variations of the periodicity with $n \times a_p$, b ranging between 4 and 6. Such a defect results in elongated superstructure reflections and streaking along **b*** as shown in the ED pattern (Fig. 10a). The corresponding [100] HREM image (Fig. 10b) shows that [001] rows of darkest spots corresponding to Hg(Bi) and Sb columns are replaced by brighter rows (white arrows). Such defects which modify the periodicity along **b** are also visible in [001] images (Fig. 4a, curved arrow). They can be easily interpreted

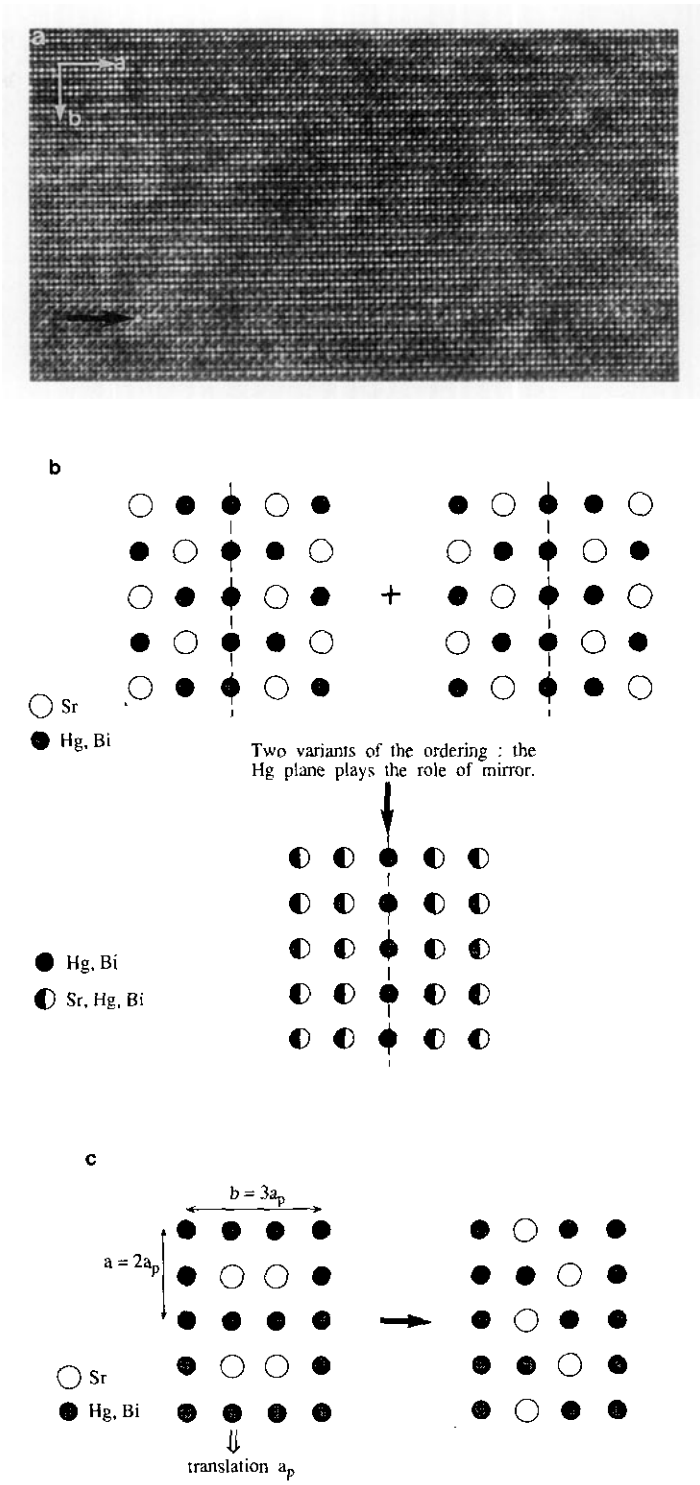

FIG. 9. (a) [001] image; the contrast of staggered white dots characteristic of the ordering feature is not always perfectly observed (left part of the image). This can be explained by a translation of two successive layers (see model in Fig. 9b) or of only one layer out of two as shown by the straight black arrow (see also Fig. 9c). (b) Model of the translation of two successive rows in the $[HgBiSrO_3]$ layer; the superposition of layers, already translated, leads to an even contrast. (c) Translation of one single row with regard to the other. The stoichiometry remains unchanged in such defective areas.

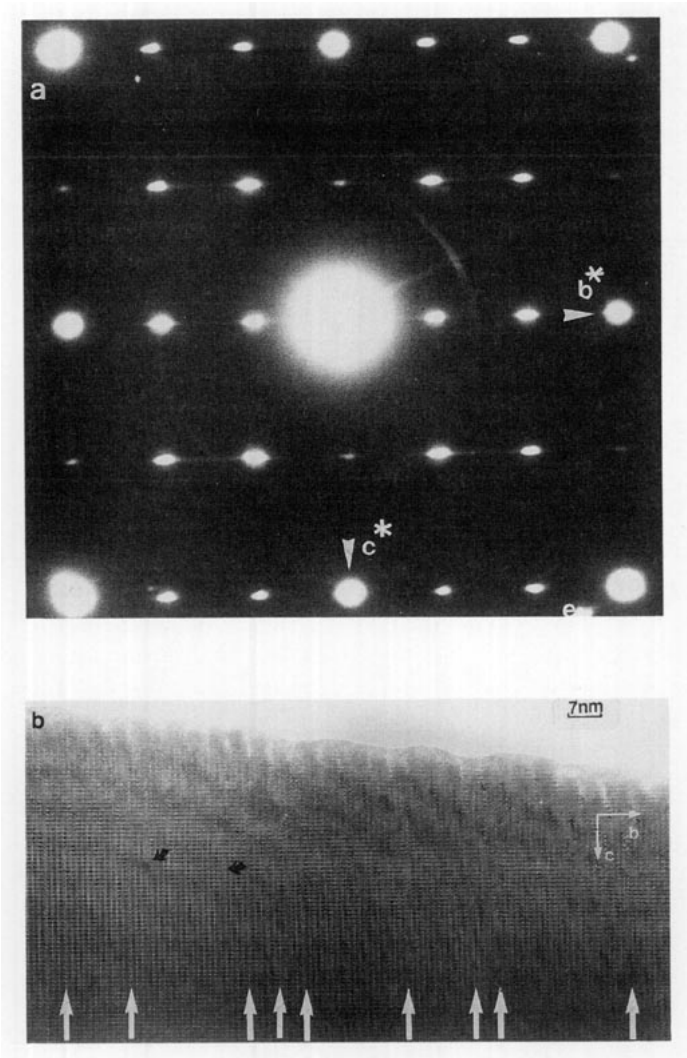

FIG. 10. (a) [100] ED pattern of a defective crystal where streaks are observed along **b***. (b) Corresponding [100] images. A local variation of the periodicity is observed along **b** (see white arrow). Changes of the cation distribution along **c** are also sometimes observed (curved arrows). (c) Idealized model of an $n = 4$ local superstructure projected on to (001).

by the existence of an additional mixed Hg(Bi)/Sr plane as shown in Fig. 10c. In such a case, the stoichiometry is modified with a Hg(Bi)/Sr ratio equal to 5/3. Note that the defect is not always extended along the whole crystal but can be interrupted (curved arrow in Fig. 10b).

CONCLUDING REMARKS

A complex ordered 1201 type structure has been isolated for the first time, that shows the ability of strontium to accomodate mercury or bismuth sites, and antimony to occupy the copper sites. There is no doubt that in such a structure the two ordering phenomena are correlated. The characterization of different ordering modes in the two types of layers is in progress. This study opens the route to the investigation of new ordered copper-based intergrowths.

REFERENCES

1. J. G. Bednorz and K. A. Müller, *Z. Phys. B* **64,** 189 (1986).
2. B. Raveau, C. Michel, M. Hervieu, and D. Groult *in* "Crystal Chemistry of HTC Superconductive Cuprates." Springer-Verlag, Berlin 1991.
3. S. N. Putilin, E. V. Antipov, O. Chmaissen, and M. Marezio, *Nature* **362** 226 (1993).
4. A. Schilling, M. Cantoni, J. D. Guo, and R. Ott, *Nature* **363,** 56 (1993).
5. S. N. Putilin, E. V. Antipov, and M. Marezio, *Physica C* **212,** 266 (1993).
6. E. V. Antipov, S. M. Loureiro, C. Chaillout, J. J. Capponi, P. Bordet, J. L. Tholence, S. N. Putlin, and M. Marezio, *Physica C* **215,** 1 (1993).
7. A. Maignan, G. Van Tendeloo, M. Hervieu, C. Michel, and B. Raveau, *Physica C* **212,** 239 (1993).
8. C. Martin, M. Huvé, G. Van Tendeloo, A. Maignan, M. Hervieu, C. Michel, and B. Raveau, *Physica C* **212,** 274 (1993).
9. D. Pelloquin, C. Michel, G. Van Tendeloo, A. Maignan, M. Hervieu, and B. Raveau, *Physica C* **214,** 87 (1993).
10. F. Goutenoire, P. Daniel, M. Hervieu, G. Van Tendeloo, C. Michel, A. Maignan, and B. Raveau, *Physica C* **216,** 243 (1993).
11. A. Maignan, C. Michel, G. Van Tendeloo, M. Hervieu, and B. Raveau, *Physica C* **216,** 1 (1993).
12. D. Pelloquin, M. Hervieu, C. Michel, G. Van Tendeloo, A. Maignan, and B. Raveau, *Physica C* **216,** 257 (1993).
13. M. Hervieu, G. Van Tendeloo, A. Maignan, C. Michel, F. Goutenoire, and B. Raveau, *Physica C* **216,** 264 (1993).
14. F. Goutenoire, A. Maignan, G. Van Tendeloo, C. Martin, C. Michel, M. Hervieu, and B. Raveau, *Solid State Commun.* **90,** 47 (1994).
15. C. Martin, M. Hervieu, G. Van Tendeloo, F. Goutenoire, C. Michel, A. Maignan, and B. Raveau, *Solid State Commun.* **93,** 53 (1995).
16. M. Huvé, C. Martin, G. Van Tendeloo, A. Maignan, C. Michel, M. Hervieu, and B. Raveau, *Solid State Commun.* **90,** 37 (1994).
17. C. Martin, M. Hervieu, M. Huvé, C. Michel, A. Maignan, G. Van Tendeloo, and B. Raveau, *Physica C* **222,** 19 (1994).
18. G. Van Tendeloo, M. Hervieu, X. F. Zhang, and B. Raveau, submitted for publication.
19. D. B. Wiles and R. A. Young, *J. Appl. Crystallogr.* **14,** 141 (1981).
20. R. D. Shannon, *Acta Crystallogr. Sect. A* **32,** 751 (1976).